Available online at www.sciencedirect.com

ScienceDirect

Advances in Space Research 75 (2025) 6944–6959

ADVANCES IN SPACE RESEARCH (a COSPAR publication)

www.elsevier.com/locate/asr

Feasibility of using CubeSats and small detectors for in-situ space debris and cosmic dust flux measurement

Luke T. Cornwell, Mark J. Burchell, Penelope J. Wozniakiewicz *

Centre for Astrophysics and Planetary Science, School of Physics and Astronomy, Univ. of Kent, Canterbury, Kent CT2 7NH, United Kingdom

Received 17 January 2024; received in revised form 31 May 2024; accepted 21 June 2024
Available online 25 June 2024

Abstract

Impacts on spacecraft by mm-sized debris in Earth orbit can have severe consequences including loss of a spacecraft and generation of more debris. This hazard and potential mitigation are discussed herein, and the risk of an impact (the product of flux and damage) is found vs. size. Reduction of the future flux of mm-sized debris by de-orbiting life-expired space vehicles, only reduces, not eliminates, this hazard. It is thus vital that the flux of mm-sized objects in orbit is well defined, but this requires on-orbit determination. To provide statistically meaningful debris flux data, large detection areas are traditionally required. CubeSats could host debris detectors, but only have small surface areas, and the data from many would be required. Accordingly, flux data from historic small space exposed surfaces are compared herein to MASTER flux model predictions, with good agreement for exposure times of just a few years, demonstrating a viable method to determine the debris flux. The cost of a network of CubeSat mounted impact detectors is also estimated found, and, for fleets of order 100 CubeSats, is comparable to the traditional single large satellite mounted instrument.

Keywords: Space debris; Impact; Low Earth Orbit; CubeSat

1. Introduction

Anthropogenic objects in space arise from human activity. Space debris has been a growing threat (Liou and Johnson, 2006) to other spacecraft ever since the first launches into space. Active spacecraft and satellites that continue to fulfil a purpose are not considered debris. However, small parts that break off such objects (such as paint flakes), or are emitted by them (e.g., aluminium oxide spheres produced in solid rocket motor burns, see Wozniakiewicz and Burchell, 2019), are debris. Similarly, if the spacecraft fails, or reaches its end-of-life, it transitions to a non-operational state and becomes a piece of large debris – this includes rocket stages used to boost spacecraft to higher orbits or beyond Earth orbit. Spacecraft can also undergo fragmentation due to internal events such as an explosion of a battery or combustion of un-used propellant. External events can also cause a similar fate, such as impact by a cm-sized object (natural or anthropogenic in origin). In most cases this is accidental, but in some cases, such disruptive impact events are intentional, designed to test anti-satellite weaponry. Whatever the cause, the result is a shower of small debris fragments that spread out in orbit. Indeed, impact by a small object of whatever origin, can result in a sudden end-of-life failure of a satellite, transitioning it into debris status. Impacts can also result in damage to the surface of a spacecraft that can liberate multiple pieces of small debris, in effect a natural multiplication effect of the total number of debris fragments in space. Thus, the debris population is not static in number, it evolves continually. Once liberated, its orbital motion is determined by its initial orbit and the result of

* Corresponding author.
E-mail addresses: ltc7@kent.ac.uk (L.T. Cornwell), p.j.wozniakiewicz@kent.ac.uk (P.J. Wozniakiewicz).

https://doi.org/10.1016/j.asr.2024.06.058
0273-1177/

external influences (solar radiation pressure, atmospheric aero-drag if in a low orbit, etc.) and thus changes with time. The result is that tracking and monitoring this debris population is a constant issue (Liou and Johnson, 2006; ESA Space Debris Office, 2023a, 2023b; National Research Council, 2011; NASA, 2021).

The debris population has been growing at a significant rate in recent years, due to the increased demand for satellite services in today's society, and the emergence of commercial launch providers. According to ESA's, 2023 annual space environment report (ESA Space Debris Office, 2023a), there were $\sim$ 8000 trackable objects in Earth-orbit in 1997, $\sim$9000 in 2007, $\sim$15,000 in 2011, and more than 32,000 in 2023. Trackable debris, is that which is large enough to be reliably tracked from earth, i.e. traditionally given as $\sim$ 10 cm or greater (Hamilton et al., 2017), but this limit has now been reduced by beam-park radar campaigns to around 1 cm (Muntoni et al., 2021). However, in space a powerful maxim is that large is rare and small is frequent. Thus, the situation is far worse than it appears because there are even more debris objects $<$ 10 cm that cannot be tracked. Through statistical modelling, ESA has predicted that, in mid-2023 (ESA Space Debris Office, 2023b), there were 36,500 objects $>$ 10 cm in orbit, $1x10^6$ objects sized from 1–10 cm, and $130x10^6$ objects sized from 0.1–1 cm.

Material in space can originate from both human related activities (i.e., space debris) and natural sources. At different sizes, one source or another can dominate the total flux. The flux also depends on the position and time in space that are under consideration. The natural flux is dominated by dust and small particles that originate mostly from asteroids and comets. These arrive at the Earth as a mixture of a continuous background flux, plus specific periods of elevated flux due to the passage of the Earth through dust streams originating from the trails of dust ejected from comets on their passage around the Sun in the inner solar system (Grün et al., 2001; Wozniakiewicz, 2017; Wozniakiewicz and Burchell, 2019).

Separating hazardous objects into cosmic dust vs. anthropological debris can be difficult. Active spacecraft are reassigned as debris at their end-of-life but still need to be tracked. Older disused vehicles can be forgotten, and when re-found, the new orbit can be traced backwards in time and compared to orbits of old spacecraft/upper stages and a match made. Larger trackable fragments from spacecraft can have their orbits plotted backwards in time, identifying possible sources. This does not work for mm-scale, non-trackable objects found in impact experiments. Here, separation into cosmic dust or debris can be done statistically, if the detector viewing direction is known, i.e. a likely origin in deep space (cosmic dust) vs. a co-orbiting source (debris) and the fluxes assumed to be dominated by one type of impactor or another. Individual particle assignments of a natural vs. anthropological origin require orbital determination (speed and direction). It is also possible to measure impactor density (from the object size and mass assuming a spherical shape), and compare to the densities of likely sources in that orbit.

In this paper a series of related questions are considered. First we find the typical risk to a spacecraft in Low Earth Orbit (LEO) arising from impact by a given sized piece of debris. This is accompanied by a discussion of mitigation strategies. Then, given that the risk is most severe in the approximately 1 – 10 mm size range, we survey available methods of measuring this flux in LEO. A lack of sensitivity in ground-based methods and a dearth of recent data from detectors in space, leads to the need for more in-situ detectors to be deployed. A comparison is then made between the cost of deploying such detectors as large area, single instruments on a single large satellite (as done traditionally in LEO) vs. hosting a fleet of small area detectors on CubeSats. To judge the scientific effectiveness of a CubeSat mounted, distributed system vs. a single large area detector, an analysis of potential flux measurements via CubeSat is then made using flux modelling software (MASTER).

2. Impact risk analysis and mitigation strategies

The degree of the hazard represented by impact by a particle of a given size can be illustrated using the long-standing method in risk analysis of taking separately the frequency of an event and its consequences. Each can then be scored for severity, and the product of the two scores defines the overall risk. For impacts in LEO, we summarise these factors in Table 1. First, we take the size range from micron to metre scale, and find a typical flux in LEO (National Research Council, 2011). This is then scored for the frequency of an impact on a scale of 1 – 10, with low frequencies (large sizes) getting a low score, and high impact frequencies (small sizes) receiving a high score. Thus for example, a flux which causes an impact per m^2 every few minutes is assessed as a 10, but impacts that occur per m^2 only once per million years (or longer) are a 1, with a sliding scale in between. Next, we list in Table 1 the typical consequences of an impact by a given size impactor. These arise due to the high collisional speed (mean debris impacts speeds in LEO, are typically in the range 7 km s^{-1} to 14 km s^{-1}, see Kessler et al., 1989). The consequences of an impact are also scored on a scale of 1 – 10, with higher scores for more severe consequences. Those consequences which are negligible would be a 1. Our lowest assigned score here is a 2 for chemical erosion, which can have long term consequences and needs to be thought of (indeed, in very low altitude orbits this risk can be higher and protective coatings need to be applied to avoid the accumulation of damage, e.g. Dignam et al., 2022). A high score of 10 for consequence is limited to impacts which disrupt the target body, producing more debris, thus worsening the problem by further polluting the environment. Again, a sliding scale between these limits is applied to intermediate degrees of damage. The product is then found and colour coded for overall risk (green is low

Table 1
Calculation of risk associated with impacts in LEO. The frequency is taken from Fig. 1. The scores for frequency and consequence are multiplied to give the overall risk. The overall risk is then colour coded into 5 bands (red the worst, green the least). The resulting risk is also shown on the flux in Fig. 1.

Size (mm)	Frequency (m^{-2} yr^{-1})	Score for frequency	Consequence	Score for consequence	Total risk score
10^{-3}	10^{5}	10	Implantation can occur leading to chemical erosion of surfaces	2	20
10^{-2}	5×10^{2}	9	Damage to fine optical components (e.g. mirrors, detectors). Penetration of thin films.	3	27
10^{-1}	10^{1}	8	Damage to exposed cables, pipes, windows, etc. Penetration of thin plates. Penetration of visors on spacesuits.	4	32
1	6×10^{-3}	5	Damage to solar cells, penetration of walls, damage to interior starts to occur. Penetration of body of spacesuit. Severing of cables.	7	35
10	5×10^{-6}	3	Penetration into interior of a spacecraft with increasing damage.	9	27
100	10^{-6}	1	Disruption of entire spacecraft, generation of significant quantities of new debris.	10	10
500	5×10^{-7}	1	Breakup of large structures (e.g. space stations)	10	10

risk, red is highest risk). A peak in the combined score occurs at around 1 mm in size. We next plot in Fig. 2, the typical LEO flux (National Research Council, 2011) vs. debris size and colour code each region as per Table 1, where mm-sized space debris can be seen to be the major impact risk for spacecraft in LEO (NASA, 2021; Furumoto and Sahara, 2020).

At larger sizes still, metre-scale and above, it is whole spacecraft that are the impact hazard. Whilst this has traditionally been low frequency, it is the case that as more spacecraft populate a region of space, this flux will increase. It should be noted that the frequency of impacts by larger objects is reduce-able by collisional avoidance manoeuvres, which rely on tracking of the objects. This is not possible with smaller (mm-sized) objects that are not trackable.

Mitigation of the risk can follow one of two paths, either minimising the consequences of an impact or by reducing the frequency (or a combination of both), see NASA-DM (2023) and IADC-2023 (2023) for example policies. The

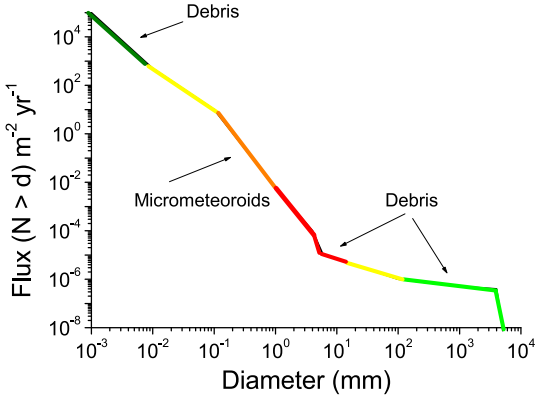

Fig. 1. Example total particle flux in LEO (below 600 km altitude). The curve has been adapted from Fig. 2.1 in (National Research Council, 2011), and colour coded for severity of risk as per Table 1. The main source (debris or meteoroid in each size regime is indicated (again taken from National Research Council, 2011). The size region around 1 – 10 mm size (coded red) can be seen to pose the greatest threat, due to the combination of frequency and consequence of impact.

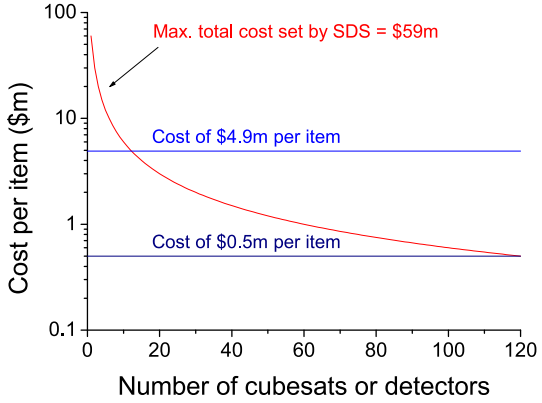

Fig. 2. The cost per detector plotted vs the number of detectors. The red line is the upper bound such that the cost of a network of multiple detectors does not exceed the cost of a single, large area detector, SDS ($59 m when inflated to 2023 values). The horizontal lines show the cost per item for the Armadillo detector ($4.9 m, Brumbaugh et al., 2012) in 2013 (inflated to current values), and an estimate of current (2023) cost for ODIN ($0.5 m, ODIN Space, 2023). The fall of an order of magnitude in the unit cost over the last decade, has enabled an increase in fleet size from 12 to 118, without exceeding the cost of SDS.

consequences can be reduced in several ways. Thin layers of material (e.g. multi-layer insulation) can act as a shield for smaller impacts (<100 μm), and bumper shields (dual walled rigid structures with a central empty region) can provide a degree of protection up to mm-scale. For mm- to cm-scale impacts, however, bumper shields can fail (with exact penetration limits depending on the composition of the shielding layers, the interlayer spacing and thickness of the rear layer for example) and material (the projectile, intact or disrupted, along with displaced material from the first layer) can penetrate the second layer into the interior. Improvement in shielding can be achieved, but at the cost of increased volume and mass. Other attempts to improve the performance at this critical mm-scale include "stuffed" bumper shields, where an extra layer (possibly woven cloth such as Nextel) can be added to the shield (e.g., Tuzzolino et al., 2003), or gels such as shear thickening fluids can be placed in the empty central region (e.g. Warren et al., 2021). Explicitly shielding vulnerable components with layers of metal can also occur, or spacecraft design can take vulnerabilities into account and place sensitive components (e.g. pipes, cables) behind other structural components. An example of this is the redesign of the space shuttle in the 1990 s, one of whose goals was to minimise the hazard due to impacts in space, and which was found to have subsequently prevented damage from an on-orbit impact which would have required a rapid termination of flight STS128 (NASA ODQN, 2010). At the International Space Station (ISS) in recent years there have been several incidents thought to be due to impacts. For example, in Dec. 2022, the Russian Souyz-MS-22 docked to the ISS suffered a loss of coolant after a putative micrometeoroid impact (TASS, 2023).

However, there are limits to shielding. As stated, the extra mass involved in bumper shields, hardening of vulnerable components etc., will drive up both construction and launch costs. In general, if a known direction has a greater flux risk and some part of the spacecraft a greater vulnerability, design of the layout of the vehicle combined with control of the spacecraft's attitude can protect more vulnerable components, provided this does not impede operational performance. However, for some components, a view of space is essential, so shielding and attitude control are not always viable solutions. There are several examples of impact damage on space telescopes for example. The NASA James Webb Space Telescope, JWST, (launched 2021 at a cost of $9.7bn, of which $8.8bn was development and $0.86bn for 5 years of operations, see (NASA FY, 2022), has already suffered impact damage on its main optical system (in its first 11 months of operations at the Sun-Earth L2 Lagrange point, the JWST suffered 14 micro-meteoroid impact events, see Menzel et al., 2023). None of the impacts on the JWST caused damage sufficient to degrade the instrument resolution outside its design parameters, but one was sufficiently concerning that, a recommendation was made to orient the JWST to avoid directions of view of high impact risk, thus reducing slightly its scope of operations. Similarly, X-ray telescopes are sensitive to impact damage (e.g., Strüder et al., 2001; Carpenter et al., 2008). In this case, grazing incidence of impactors on the X-ray focussing mirrors, can focus ricocheting projectiles or impact ejecta onto the sensitive CCD devices, which measure the X-rays, causing damage. Whilst individual impacts may cause minimal/local damage on the CCD, the cumulative effects may threaten mission longevity. Indeed, due to the focussing effect, the effective collector area for micro-meteoroids is enhanced, thus increasing the frequency of impacts, i.e. it is not the CCD detector area that determines the flux, but rather the area sampled by the collecting mirrors.

Minimisation of the hazard due to impact avoidance strategies is possible. As well as sporadic events, meteoroids can come in streams whose arrival can be predicted. The Perseid meteoroid stream for example, is an annual event, and impacts from Perseids are thought to have damaged at least two satellites. Landsat-5 may have been struck by a Perseid in 2009, and control of the craft was lost for several days before normal operations resumed (Cooke, 2014), and in the case of the Olympus satellite in 1993 this was an end of life event (Caswell et al., 1995). Spacecraft cannot avoid these meteoroid streams per se, however, similar to the JWST, they can orient themselves to protect sensitive components.

For impacts by > mm-scale objects, the consequences become so severe that shielding or re-orientation of spacecraft provide little mitigation. Instead two solutions are required, either avoidance manoeuvers (for trackable larger impactors) or reducing the flux of the offending objects (NASA ODQN, 2020). The former strategy, avoidance, is increasingly used by space assets (e.g., the ISS and individual satellites). However, this places a strain on propellant consumption, is disruptive of operations and involves ever-increasing control issues over large constellations of satellites. Indeed, as the number of satellites increases, this may no longer be a viable option. For example, between 2019 and July 2023, the Starlink constellation had to carry out over 50,000 collisional avoidance manoeuvers, and this is rising, with 25,000 alone in the six months to end June 2023 (Space.Com, 2023).

Therefore, the second option, reducing the flux, becomes necessary. Two paths are being followed; one is that all space vehicles must de-orbit within a fixed period of their end-of-life. The other is to actively remove defunct space vehicles. A variant on these approaches is to prolong the lifetime of satellites by refuelling in-orbit, thus reducing the number of satellites required over long periods. Studies show that de-orbiting 90 % of spacecraft within 25 years of their end-of-life and removing an additional 5 dead and non-responsive vehicles each year, will reduce (but not eliminate) the rate of growth of the debris environment (NASA, 2021). However, whilst over the last decade NASA has managed a 96 % compliance with deorbiting strategies, world-wide the figure is 20–30 % (NASA, 2021), and technologies to de-orbit dead vehicles are only

now being demonstrated (NASA SOA, 2022). However, in this context, compliance only means that at its end of mission, a spacecraft is at a sufficiently low altitude that it will re-enter the atmosphere within a further 25-year period. To improve this situation, in 2022, the US Federal Communications Commission (FCC) introduced a new rule that requires de-orbiting within 5 years of end-of life for all US launched commercial satellites or for satellites whose services are offered in the US market (FCC, 2022).

Whilst de-orbiting is essential, it is not in itself sufficient to avoid all future impact hazards from larger impactors. Spacecraft can still undergo unexpected disruptive events that can generate large numbers of smaller fragments. They will also undergo impacts by meteoroids, which can cause damage and mission failures. Meanwhile, the growth in the number of active satellites in orbit (i.e. in mega constellations) will add to the total population at larger sizes. Indeed, whilst we transition to a new era of de-orbiting more defunct objects, there will be several decades of vulnerability. Separate to this, the issue of how to enforce de-orbiting strategies on all players is a complicated one. The nation from whose territory a space vehicle launches carries liability for the consequences of its launch. However, enforcing this on some countries may prove difficult, and indeed clearly showing that an mm-sized piece of debris from a known source was the cause of damage to a spacecraft seems difficult.

Furthermore, the willingness of some countries to carry out weapons testing which involves damaging or destroying satellites, may seem reckless in light of modern appreciation of the risk debris poses. During the late 20th century, both Russia and the United States developed and tested anti-satellite weapons. An example of the consequences for space debris is provided by the 1985 US destruction of an old satellite (Solwind P78-1) at an altitude of 525 km (Anz-Meador et al., 2022). The last piece of trackable debris was reported to have re-entered the Earth's atmosphere in 2004, some 19 years later. In this century alone, anti-satellite weapon tests include China's destruction of its the Fengyun-1C satellite (altitude 865 km) in 2007, creating the largest known human-sourced cloud of space debris (Pardini and Anselmo, 2009, Kelso, 2007), Russia destroying Cosmos-1408 in 2021 (Pardini and Anselmo, 2023) and India destroying a satellite in 2019 (Ahmad, 2021). Separately, in 2007, the US destroyed a mal-functioning satellite (USA-193) at low altitude to avoid the risk of a large, intact object undergoing an un-controlled re-entry whilst still containing dangerous amounts of propellants (Johnson, 2021). The debris resulting from these events has a lifetime that depends on altitude, and low altitude debris mostly clears within months. The Cosmos-1408 breakup for example, created a debris field at altitudes from 440 – 520 km, which at times has been deemed to pose a threat to various satellites and even the ISS. Within 2 years, about 5/6th of the trackable debris from this break-up event had re-entered. While fragments of satellites destroyed at lower altitudes (less than 300 km) typically decay within months, some fragments can be thrown into higher orbits and persist for longer.

Mitigation alone is thus insufficient, and monitoring of the space environment is vital. Further to the space debris population, there is also naturally occurring cosmic dust in the near-Earth environment (Wozniakiewicz, 2017). As already stated, this is dominated by interplanetary dust that is thought to originate from asteroids and comets, and measurements of these particles provides significant scientific insight into the constituents and conditions of the parent bodies (Grün et al., 2001, 2019). Direct measurements of the particles are thus required in order to: understand the threat posed by non-trackable debris and its evolution vs. time, enable the development of adequate shielding, and address the problem of space debris in space sustainability.

3. In-situ impact detector technologies

In-situ, 'active' dust detectors (i.e. those that measure characteristics of particles 'live' as they impact/are collected by a detector) have been flown in space since the beginning of the space age, initially to identify the risk to space vehicles posed by cosmic dust and then to measure the flux at various locations in the solar system (e.g., Grün et al., 2001). Such detectors can be based on a range of technologies which send data back to Earth in real-time so the hosting spacecraft does not have to be retrieved (i.e. for flux measurements by laboratory study of cratered surfaces). Example detection methods have traditionally included acoustic (piezoelectric) detection, such as the 'Impact Sensor' subsystem of the Grain Impact Analyser and Dust Accumulator (GIADA) instrument flown aboard the Rosetta mission to Comet 67P (Sordini et al., 2018). Impact induced plasma detection is also used, such as the Impact Plasma and Momentum subsystem of the Dust Impact Detection System (DIDSY-IPM) flown aboard the Giotto probe to comet 1P/Halley (McDonnell, 1987). Detectors can also combine several methods, for example, the Debris In-Orbit Evaluator (DEBIE) dust detector (deployed in Earth orbit in 2001) used both acoustic and plasma detection to measure the dust flux in LEO for micron-sized particles (Schwanethal, et al., 2005). A summary of many examples of different types of impact detector carried on various satellites, or which have been tested in the laboratory, is given in Table 2. The key parameters given include details of the impactors the detectors are sensitive to (e.g. size, speed, etc.), and their active areas. Some of the references quoted in Table 2 also give details of total mass, power consumption, etc., but these are not always widely available. It is notable that a wide range of detector technologies is now available, and that many have been developed, tested and, in some cases, even deployed in the last 10–15 years.

As discussed in Section 2, due to their large population and consequence of impact, mm to cm-sized debris is considered the greatest threat to most spacecraft in LEO.

Table 2
Example traditional impact based detectors/technologies to measure space debris/interplanetary dust in-situ in Earth orbit. The impactor size column has been colour coded to reflect the hazard assignment in Table 1, with red indicating detectors sensitive to the most critically sized debris in terms of impact risk. The number of detectors of the given size that must be deployed to achieve a benchmark 1 m^2 exposed area is given, and can be seen to range up to the 100 or so. Impactor speed and direction are required to determine the orbit and separate into a likely cosmic dust or debris origin. The impactor size the detectors are sensitive to is usually given as a range, or an upper limit, where single values are given these are the sizes tested in the reference given. (See above-mentioned references for further information.)

Name/Technology	Impactor size (mm)	Impactor Speed Accuracy	Impact direction	Active area (m^2)	Number to achieve 1 m^2 active area	Ref
SDS: Acoustic sensors+resistive grid/thin films (25μm)	0.075 – 1+	±18% (at 7 km s^{-1})	±3% (average), 10% (maximum)	1	1	Hamilton *et al.*, 2017
ODIN: Acoustic sensors/thin film (25μm)	0.3 – 1.5	±4% at 2.75 – 5 km s^{-1}	±1.2°	0.06	17	ODIN Space, 2023
SDS style acoustic sensors/thin films (12.5μm)	0.05 – 1+	±1% at 5 km s^{-1} and 2% at 10 km s^{-1}	Not stated, but similar to Hamilton *et al.*	0.058	17	Cornwell *et al.*, 2023
Impact flash on solid surface - laboratory only (state of art)	10^{-5} - 10^{-3}	±6.5 km s^{-1} independent of impact speed	N/A	0.13	8	Goel *et al.*, 2017
GORID (impact ioisation)	5×10^{-5} – 2×10^{-2}	Factor of 1.6 - 2	±70°	0.1	10	Drolshagen *et al.*, 1999, Graps *et al.*, 2007
DEBIE (impact ionisation/pzt)	$(1.5 – 3) \times 10^{-3}$	Factor of two	N/A	0.01	100	Schwanethal *et al.*, 2005.
DISC (impact ionisation/pzt)	0.002 – 0.2	N/A	N/A	0.007	143	Della Corte *et al.*, 2023.
SOLID (solar panel/resistive grid)	0.1 - 10	N/A	N/A	0.0755	13	Bauer *et al.*, 2016; Bauer 2021
SPADUS (PVDF depolarisation TOF)	0.0033 – 0.2	Factor of two	Typically ±50° (at normal incidence)	0.0576	17	Tuzzolino *et al.*, 2001.
PDVF (depolarisation) - laboratory only (state of art)	3.2	±3% at 1 km s^{-1}	±2° (at normal incidence)	0.0025	400	Liu *et al.*, 2021
ADLER/APID1 (array of piezo foils)	<0.1	N/A	N/A	0.0865	12	Groemer *et al.*, 2023
ADLER/APID2 (piezo ceramics on glass fibres panels)	Not stated	N/A	N/A	0.50	2	Austrian Space Forum, 2023.
IKAROS (solar sail/acoustic sensors)	0.004 – 0.056	±40% at 10 km s^{-1}	N/A	0.54	2	Hirai *et al.*, 2014.
EQUULUS (MLI/acoustic sensors)	0.004 - 1	N/A	N/A	0.0439	23	Funase *et al.*, 2020.
ASTERISC (thin film/acoustic sensor)	<0.001	N/A	N/A	0.1	10	Ishimaru *et al.*, 2021.
Horyu-II (resistive wires on PCB)	0.1 - 0.6	N/A	N/A	0.0081	123	Faure *et al.*, 2013.
DEDRA (plasma ionisation detection)	0.001 – 0.040	Factor of 1.5	Not stated	0.0082	122	Oikonomidou *et al.*, 2022.

Unfortunately, measurements of the dust flux in LEO in the size range of ~ 100 μm to a few mm, is uncertain or based on old data, leaving the flux poorly constrained (Wozniakiewicz and Burchell, 2019). Thus, in recent years there has been increased research in developing detectors optimised for mm-sized debris (e.g. Hamilton et al., 2017, Liou et al., 2006, Schimmerohn et al., 2021, Cornwell et al., 2023), and these are also summarised in Table 2. The unfortunate failure of the NASA SDS soon after deployment (Anz-Meador et al., 2019) prevented data being obtained in this critical size range, but this data-gap needs to be filled.

4. CubeSats as platforms to host impact detectors: Plausibility and costs

A change is taking place in the space sector known as the "small satellite revolution", where, for many applications, small and relatively cheap satellites are being chosen in favour of more traditional larger satellites. In particular, nanosatellites (satellites with a mass $\leq$ 10 kg) are becoming very popular, due to the improved launch availability for such small satellites, and the modular design standard of the CubeSat. To reduce costs, CubeSats have to conform to criteria governing their form factor and mass (CalPoly, 2022). To achieve this, the volume of a CubeSat is based on the CubeSat unit, known as a 'U'. Each 1U is a cube with 10 cm edges (i.e., 10 cm × 10 cm × 10 cm, with volume 1000 cm^3) with an associated mass of originally typically 1 kg but more recently up to 2 kg. Examples of common CubeSat sizes are 1U, 1.5U, 3U, and 6U; with a typical mass of 1 kg, 1.5 kg, 3 kg, and 6 kg, respectively. This standardisation allows companies, such as NanoAvionics and AAC Clyde Space, to produce CubeSats using "Commercial Off-The Shelf" (COTS) components and standardised structures. These factors make CubeSats relatively cheap to produce and quick to market/launch, thus increasing accessibility to space. Unfortunately, ease of access to space coupled with often relatively short operational lifetimes and a lack of end-of-life de-orbiting strategies, means that CubeSats can contribute to the concerning levels of anthropogenic debris in Earth-orbit. However, they can also support solutions to space sustainability as well as providing the more traditional useful aspects of CubeSats, from educational purposes and technology demonstration, to improved spatial and temporal resolutions.

The recent move towards using CubeSats has led to research on developing dust impact detectors that are small enough to be carried by CubeSats, such as the development of the Dust Impact Sensor and Counter (DISC, Della-Corte et al., 2023) based on the GIADA technology, due to fly aboard the ESA's Comet Interceptor mission (Snodgrass and Jones, 2019) and proposed for application to CubeSats. Another example is the space dust impact detector flown aboard the technology demonstrator nanosatellite Horyu-II, with a detector mass of ~ 30 g, size of 90 mm x 90 mm and cost of ~€200.00 (Faure et al., 2013). Alternatively, SOLID, the SOLar panel based Impact Detector (Bauer et al., 2016) uses copper wire grids (which experience a change in resistivity when wires are severed in impacts) inserted into solar panel substrates to provide data on impacts (instrumenting the solar panels provides large collection surface areas). SOLID was first launched for on orbit verification in 2017 on the nanosatellite TechnoSat, and is planned for another verification mission in 2024 aboard CompactSat (Bauer, 2021). Other CubeSat missions for debris detection are also underway, including for example: the 3U CubeSat 'Attitude Related Manoeuvres And Debris Instrument in Low (L) Orbit' (ARMADILLO), flying the Piezoelectric Dust Detector (PDD) instrument, which launched in June 2019 and re-entered on August 2022 (Brumbaugh et al., 2012). There are also the 3U CubeSat 'Austrian Debris Detection Low Earth (orbit) Reconnoiter' (ADLER-1), flying both the Austrian Particle Impact Detector (APID, using PZT impact detection), which launched in January 2022 (Groemer et al., 2021); and the 6U ADLER-2, flying APID-2, which launched April 2023 (Austrian Space Forum, 2023). Both models of ADLER are currently in orbit (mission updates available at Austrian Space Forum, 2023). There are more CubeSat missions under development, such as e.Cube (Columbo et al., 2021), STRATHcube (Creed et al., 2021), and Move-III (Oikonomidou et al., 2022). Again, see Table 2 for details of various types of impact detectors on these spacecraft. What is clear is that CubeSats are now being used to host dust impact detectors.

This move to Cubesats can be considered analogous to the 1990s NASA mantra "faster, cheaper, better". Whilst

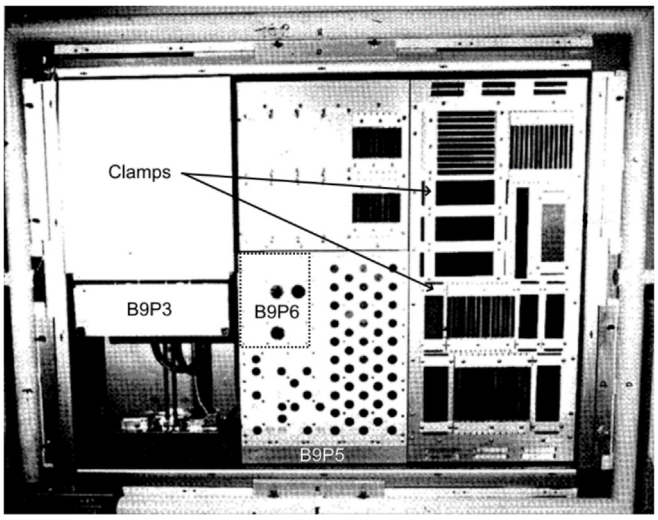

Fig. 3. Tray B9 post LDEF de-integration after retrieval from orbit (Humes, 1993). The three small plates used for this investigation are shown labelled with the ID numbers (B9P…) assigned to them in the original study. The outer edge of plate B9P6 has been marked with a dashed line. Two of the small plates used as 'clamps' are shown (See et al., 1990).

Table 3
Data from a crater survey (Humes, 1993) on aluminium plates from Tray B9 of the LDEF mission, with an area < the largest face of a 6U CubeSat (0.06 m^2). The area of each plate, number of craters with a crater lip diameter (D_r) ≥ 500 μm and ≥ 1000 μm, and their corresponding flux are shown. The final row represents a total over all cells. Accumulated flux was calculated using the total area, relevant total number of impacts, and the duration of space exposure of 5.75 years. A single row represents the 28 small plates used as clamps ('clamps') that did not receive any impacts. Note that the combined area and exposure time cancel to give a flux equal to the number of craters.

Plate ID	Area (m^2)	Number of Craters		Flux (m^{-2} y^{-1})	
		$D_r \geq 500$ μm	$D_r \geq 1000$ μm	$D_r \geq 500$ μm	$D_r \geq 1000$ μm
B9P3	0.044	4	1	15.8	4.0
B9P6	0.0387	2	1	9.0	4.5
B9P5	0.0185	0	0	0.0	0.0
B9P7	1.8 $x10^{-3}$	1	0	96.6	0.0
x 28 clamps	1.4 to 4.5 $x10^{-3}$	0	0	0.00	0.00
Total/accumulated flux from 32 Plates	0.174	7	2	7	2

subsequently often slighted, this aimed to increase the return per dollar spent, and as such was successful. With CubeSats, the intention can be seen as using COTS items and technologies (at lower cost than normal space qualified components), with rapid turn-around times from conception to launch, using structures produced at scales of the hosting platforms. That this is appropriate, and faster and cheaper, does not automatically follow in all cases and needs quantification. Here, we can contrast the more traditional NASA DRAGONS/SDS large area dust detector with an approach based on use of CubeSats. The SDS was the result of at least a decade of NASA development work. In 2019, a successor was budgeted at $49 m for deployment and 3 years operation (NASA FY2022, 2022), applying a crude estimate of the cumulative annual inflation taken from the UK Office of National Statistics (UK Stats, 2023), this is equivalent to $59 m in 2023.

The costs for CubeSat based detectors can be hard to fully quantify, as this is often commercially sensitive, or costs are given for the manufacture of the instrument alone and do not include the satellite, integration and testing, launch or operations. A full cost analysis for flying an impact detector on a 3U CubeSat was performed for Armadillo (Brumbaugh et al., 2012), and suggested a cost of $1.5 m for design and construction of the detector and associated CubeSat, plus a further $2m for integration, testing, operations, etc. This gives a total cost of $3.5 m in FY2011. If we apply a crude accumulated inflator as before, of 40 % since 2011, this is equivalent to $4.9 m in 2023. Comparing costs, 12 Armadillo satellites could thus be provided for the cost of one SDS (see Fig. 2). However, costs have fallen in recent years, both for construction as COTS components are used, and as more opportunities for launch have appeared, including hosting a small payload on larger satellites or launching multiple satellites simultaneously, lowering the per unit launch cost. Current launch costs for ride-share launches, come to some $70 k/kg or less, indicating a 1U (2 kg) CubeSat launch can be obtained for order $140 k. When adding construction costs (which can be low using COTS components, say $50 k) and several years of operations (allow $100 k per year for staff and software), a complete CubeSat mission can be foreseen to cost some $500 k for a 3 year operational period. This is supported by the example of ODIN Space (ODIN Space, 2023) which has recently launched a debris-monitoring detector hosted on the D-Orbit ION satellite Savvy-Simon (D-Orbit Space, 2023). According to the ODIN website (ODIN Space, 2023), the mission will last several years, and the company raised $500 k in funding to support its activities. If all this money is associated with the current mission, this sets a mission cost per unit of $0.5 m, significantly lower than the estimates of $4.9 m from a decade earlier (Brumbaugh et al., 2012). This suggests a fleet of around 120 CubeSat mounted experiments is comparable in cost to a single SDS mission (Fig. 2).

5. Can a distributed network of CubeSat mounted flux detectors produce a meaningful combined flux estimate?

To provide meaningful statistical data, in-situ detectors need a detection area large enough to ensure they encounter a representative number of particles/impacts of the desired size within the mission's lifetime. For a 3-year mission at an altitude of 700–1000 km, a 1 m^2 detection area with an optimal pointing direction is considered a minimum (Hamilton et al., 2017). Some proposed detectors aimed for even larger detection areas e.g. the Large Area Debris Collector (LAD-C) (Liou et al., 2006), which was to have an area of 10 m^2. The SDS/DRAGONS dust detector (Hamilton et al., 2017) which launched in Dec. 2017 (and was resident on the ISS at 420 km altitude), had a 1 m^2 active area with impacts detected by acoustic sensors and resistive wires on a thin film (due to data relay failures only 25 days of on-orbit data were generated (Anz-Meador et al., 2019)). By contrast, a 1U CubeSat face has a surface area = 0.01 m^2, hence, to produce a 1 m^2 detection area, 100 individual 1U CubeSat faces would be required. Thus, to achieve areas large enough to provide statistically meaningful data, without employing area-increasing technologies, accumulation of detection area over multiple CubeSats will be required. This leaves the use of CubeSats for space debris detection with a fundamental question:

Will the accumulation of detection area over many CubeSats lead to statistically meaningful data? This is especially critical when, at the larger particle sizes (e.g. 1 mm), most individual CubeSat sized detectors will return null results in any given time interval less than a decade, thus the data set will mostly consist of zeros.

To test this, a comparison was made of the impact flux measured by a historic space mission Long Duration Exposure Facility (LDEF) (Humes, 1993) with predictions from ESA's Meteoroid and Space Debris Terrestrial Environment Reference (MASTER) software for predicting dust fluxes. Although a single spacecraft, LDEF had components that are smaller than a common CubeSat. Therefore, the actual accumulated flux from individual LDEF space exposed plates is compared to predictions from ESA's MASTER modelling software (ESA, 2023). Effectively, a set of data equivalent to that from a network of CubeSats is compared to the average flux predicted by modelling, to see if the results are comparable.

5.1. Method

The data for the impact flux on space-exposed surfaces used in the comparison came from the LDEF mission, placed in orbit April 1984 and retrieved January 1990 (see O'Neal & Lightner, 1991, for an overview of the LDEF mission). LDEF was exposed to space for 69 months and comprised of numerous trays, which were used for investigations in fifty-seven experiments. The orbit was near circular with an apogee of 480 km and a perigee of 474 km, and an inclination of 28.5°. LDEF had a three-axis gravity-gradient stabilised configuration, resulting in a known pointing direction.

Post-flight, the space exposed plates in question were donated to the LDEF Meteoroid and Debris Special Investigation Group by Wayne Slemp (NASA Langley Research Centre) from the tray at location B9 (Tray B9), and were subject to a crater survey (Humes, 1990). The plates and small strip-like plates used to fix samples to the tray (known as clamps) were made of aluminium Al6061-T6 (see Fig. 3). Only plates with an area smaller than the largest face of a 6U CubeSat (0.06 m^2) were considered here. For these small plates, only data for craters with a crater-lip diameter (D_r) of $\geq$ 500 μm were reported (Humes, 1990). The location on tray B9 of the LDEF small plates and clamps used here is shown in Fig. 3, and a list is given in Table 3, along with their area, the number of impacts observed with a $D_r \geq 500$ μm and ≥ 1000 μm, and the corresponding flux. The ID numbers are those assigned to the plates during the original crater survey, note that the clamps were assigned ID numbers of B9P7 and above. Only one clamp received an impact $\geq$ 500 μm, the other twenty-eight clamps received zero impacts $\geq$ 500 μm and are represented by a single row in Table 3.

Individual fluxes for a given size range were then calculated for each plate using the plate area and exposure time of 5.75 years. An accumulated flux was calculated by combining the total area of all the plates and the total number of craters of each size range per unit time. The flux accumulated from the total 0.174 m^2 area of small plates from Tray B9 was 7 ($D_r \geq 500$ μm) and 2 impacts m^{-2} yr^{-1} ($D_r \geq 1000$ μm).

Particle environment modelling for the comparison was carried out with version MASTER-8.0.3 of ESA's MASTER software (available at ESA, 2023c). To assess that the MASTER software was being operated correctly, a test was carried out to replicate past data produced with MASTER-8 by V. Braun (space debris engineer at ESA, responsible for developing MASTER) (Wozniakiewicz and Burchell, 2019). For this comparison only the epoch, altitude, and inclination previously used were known, the other orbit parameters were left as their default value

Table 4
Parameters input in Master and ESABase2/Debris. RAAN stands for "Right Ascension of Ascending Mode" and SRP for "Solar Radiation Pressure".

Target Orbit Settings for LDEF Simulations						
Start epoch (YYYY/MM/DD/HH)	**End epoch (YYYY/MM/DD/HH)**	**Semi-Major Axis (km)**	**Eccentricity**	**Inclination (°)**	**RAAN (°)**	**Argument of perigee (°)**
1984 04 07 12	1990 01 12 12	6854	1 x10^{-4}	28.5	0.0	0.0
Satellite Properties for LDEF Simulations						
Mass (kg)	**Cross Section (drag) (m^2)**	**Cross Section (SRP) (m^2)**	**Drag Coefficient**	**Drag Coefficient Rate (1/d)**	**Reflection Coefficient**	
9710.0	39.13	27.7	2.2	0.0	1.3	
Orbit parameters used for the ESABase2/Debris and MASTER simulations at 800 km altitude						
Start epoch (YYYY/MM/DD/HH)	**End epoch (YYYY/MM/DD/HH)**	**Semi-Major Axis (km)**	**Eccentricity**	**Inclination (°)**	**RAAN (°)**	**Argument of perigee (°)**
2023 11 01 00	2026 11 01 00	7178.0	1 x10^{-4}	98.7	0.0	0.0
Input parameters for MASTER's 'Satellite Properties' used for the propagation of future CubeSat missions and the 6U simulation in ESABase2 (mass and cross section used for the other CubeSat sizes scale accordingly).						
Mass (kg)	**Cross Section (drag) (m^2)**	**Cross Section (SRP) (m^2)**	**Drag Coefficient**	**Drag Coefficient Rate (1/d)**	**Reflection Coefficient**	
6	0.06	0.042	2.2	0.0	1.3	

(the default eccentricity is 0.001). The results of the test are of the same order of magnitude and deviated by an average of 6 %. This difference may be due to a difference in starting conditions (e.g. a differently selected population) and/or updates in the software, but is nevertheless small enough to suggest that MASTER was implemented correctly.

For the comparison to the historic data, particles in the range 10^{-6} m $\leq D_p \leq 3$ x10^{-1} m were considered. Tray B9 had a pointing direction of 8° from the LDEF velocity vector (Humes, 1993), this was replicated in MASTER with an 'orientated surface' target type pointing 8° from the velocity vector, along the Azimuth angle. The 'Debris Sources' and 'Meteoroid Sources' selected were the 'Condensed' and 'Grün (constant velocity 20 km s^{-1})' sources, respectively. The 'Target Orbit Settings' are shown in Table 4. A circular orbit (eccentricity = 0.0001) with an altitude of 476 km was assumed, the altitude at which LDEF spent most of its mission. Thus, the argument of perigee (AoP) was not applicable and set to 0.0. The similarly unknown right ascension of the ascending node (RAAN) at the time of orbit insertion was take as 0.0. This is not expected to affect results as tests showed that differing RAAN had negligible effect, as expected from MASTER's random treatment of RAAN. Orbit propagation was enabled, with the 'Satellite Properties' (Table 4). Satellite properties were based on the information in O'Neal & Lightner, 1991, and the coefficients were the default values. Where parameters or options have not been specified, it can be assumed that they were left as their default setting.

MASTER-8.0.3 was also used to model the impact flux in the current era for a circular, polar orbit with an altitude of 800 km and inclination of 98.7° (full orbit parameters are shown in Table 4), using the 'Condensed' and 'Grun (constant velocity 20 km/s)' source populations. Predictions for the impact flux on the leading edge of a 1U, 1.5U, 3U and 6U CubeSat over 3 years were made (where the CubeSat's largest face was used as the ram direction, i.e. aligned with the velocity vector and maximising the encountered debris flux). Flux predictions were extended to the total flux incident on all faces of each size CubeSat (see Fig. 5), using geometric analysis in the ESABase2 12.0.2/Debris software (license and software available from the developer Etamax Space GmbH, see FEV, 2023). The 'model selection' was chosen to match the MASTER simulation, i.e. a 'debris and meteoroid analysis' with the 'MASTER 8′ model and the Grün 'Gruen' meteoroid model. Each CubeSat was modelled as a cuboid of the appropriate size (i.e. a simple CubeSat with no deployable surfaces or components). These fluxes were then used to infer the expected time before encountering a particle of a given size, for the leading face and entire CubeSat, respectively. The satellite properties used in MASTER and ESABase2/Debris (for the 6U simulation) for the orbit propagation were taken as those for a 6U satellite, given in Table 4. Note: that future debris populations were downloaded from reference ESA, 2023c, and added to the relevant file directory in the ESABase2 data files to run these future simulations.

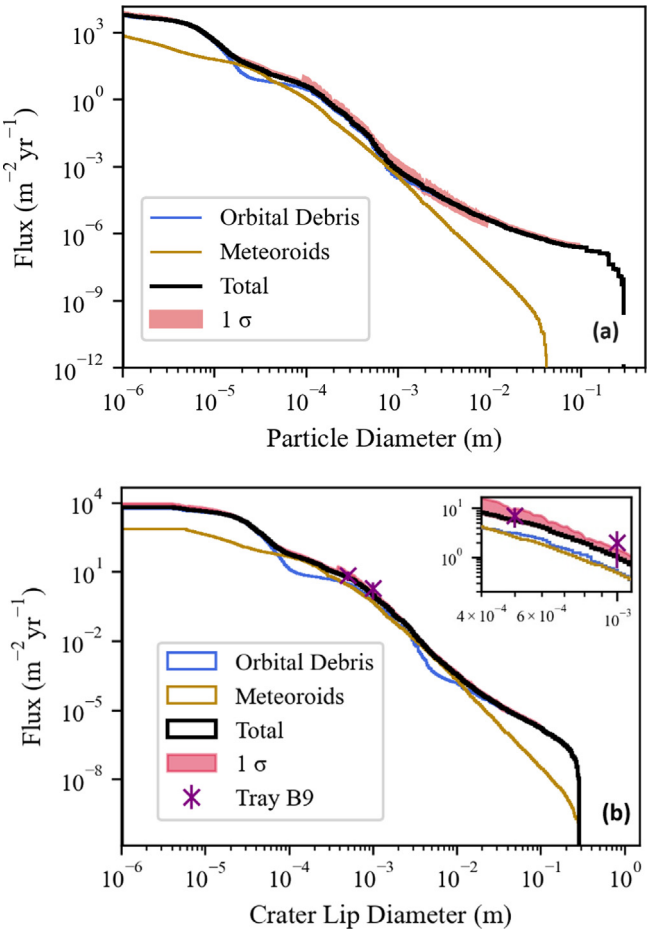

Fig. 4. **(a)** Cumulative particle flux data for particle diameter (D_p) in the range 10^{-6}m $\leq D_p \leq$ 3x10^{-1}m, for a LDEF like orbit as predicted by MASTER (orbit parameters in Table 2). The contributions from the debris and natural particles are shown separately, along with a combined total flux and the estimated 1σ variation in the total flux. There is an increase in the relative uncertainty between 10^{-4} m and 10^{-2} m, because of the poorly constrained flux for this population. **(b)** Cumulative flux data (solid lines) for craters with a given crater-lip diameter (D_r) for impacts into Al6061-T6, in an LDEF-like orbit as predicted by MASTER (orbit parameters in Table 4). Fluxes were derived from particle diameter flux data for particles in the range 10^{-6} m $\leq D_p \leq$ 3x10^{-1} m (Fig. 3), using crater scaling relationship (eq. (1)–(3). The real LDEF data (×) is also shown and is in good agreement with the prediction. The region with the LDEF data is also shown expanded (top right).

To convert incident particle size into the crater size associated with that impact (i.e., into a crater size rather than a particle size flux for comparison to the measured crater sizes on LDEF) requires use of appropriate formulae. There are many different damage equations and crater scaling relationships available in the literature, some of which are based on theory (e.g. Watts et al., 1993), but most on experiment (e.g. Cour-Palais, 1987). A study on the best damage equation to use for Al6061 (Hörz et al., 1995), found that Christiansen's damage equation (Hörz et al., 1991), (Christiansen, 1993) (modified from

the Cour-Palais equation) best fit the experimental data for hypervelocity impacts into Al6061 and is thus used here as follows to convert D_p to D_r. First the particle penetration depth (P) was found from Eq. (1). For experimental laboratory impacts into aluminium at speeds of ~ 7 km s^{-1} craters are typically hemispherical, thus the crater diameter at the original surface (D_c) relates to P as per Eq. (2) (note that (Humes, 1993) reported the depth/diameter ratio for the LDEF craters here as 0.50 to 0.56). It was later reported that LDEF craters in general typically had depth/diameter ratios ~ 0.56, but this covers a wider range of crater sizes (Love et al., 1995). Finally D_r relates to D_c according to Eq. (3).

$$P = 5.24 D_p^{\frac{19}{18}} H^{-\frac{1}{4}} \left(\frac{\rho_p}{\rho_t}\right)^{\frac{1}{2}} \left(\frac{v}{v_c}\right)^{\frac{2}{3}} \quad (1)$$

$$D_c = 2P \quad (2)$$

$$D_r = 1.28 D_c \quad (3)$$

where ρ_p and ρ_t are the density of the particle and target, respectively. v and v_c are the impact velocity and sound speed in the target material, respectively, and H is the Brinell hardness of the target material. The density of the Al6061-T6 target was taken as 2.7 g cm^{-3}, H as 90 and v_c as 5.1 km s^{-1}. Space debris and meteoroid populations were considered separately, with an average density of 2.7 g cm^{-3} and 2.5 g cm^{-3} assumed for each, and an average impact velocity of 10 km s^{-1} and 18 km s^{-1} respectively (estimated from the surface normal impact velocity data from MASTER). The average space debris density was assumed to be the density of aluminium, while the density for meteoroids was taken from Humes, 1993.

5.2. Results

Flux data produced using Master-8.0.3 are shown in Fig. 4a, for particles with a diameter (D_p) in the range 10^{-6}m $\leq D_p \leq 3\text{x}10^{-1}$m for an LDEF like orbit, with LDEF's epoch, and the same pointing direction as Tray B9. To draw a comparison between this flux and the crater-lip diameter (D_r) data from LDEF, a conversion from D_p to D_r was applied yielding Fig. 4b (the LDEF small plate flux is also shown for comparison). From Fig. 4b, we see that flux data accumulated over multiple surfaces is in good agreement with the flux predicted in MASTER. The error bars in Fig. 4b are the uncertainties outputted by MASTER that are associated with the total flux in Fig. 4a, shifted to the corresponding size population. This shift is based on the minimum crater size produced by a 1 μm debris particle impacting at 10 km s^{-1}. Thus, they represent a minimum uncertainty that does not take into consideration uncertainties related to the scaling relationship applied, the use of an average impact speed and impactor density, and the disparity between the crater-lip diameter shift for the meteoroid and debris populations.

To consider how the flux would be measured by a CubeSat in the modern era, we also modelled in MASTER the impacts on various sized CubeSats in a near polar orbit at an altitude of 800 km over a 3 year period starting in 2023 (see Method section). The resulting annual fluxes on various surfaces of a 6U CubeSat are shown as an example in Fig. 5. It should be noted that this flux covers 4 orders of magnitude in impactor size, and, as indicated in Fig. 4, it is the smaller sizes that dominate. In Fig. 5, only three faces are shown. The fluxes on the other three faces show the following trends: The anti-Ram face flux is lower than the Ram face due to the motion of the spacecraft. The –Y face has a similar flux to the Y face, and the space-point face (−Z) has a higher flux than the Earth-pointing face (Z) as it is not shielded by the Earth.

The particle flux in the size range 10^{-6}m $\leq D_p \leq 1\text{x}10^{-2}$m, incident on the ram face and entire CubeSat surface area in Fig. 5, were converted to days/impact in Fig. 6, where we see a noticeable difference in the power law fit to the data above a particle diameter of 10^{-3} m. This is reflective of the change in the underlying population from mm to cm. This is also evident in Fig. 4a where around the 10^{-3}m (mm) mark the gradient of the total particle flux flattens, even though the meteoroid population is still falling rapidly. This is likely a combination of the different production sources and processes, governing the evolution of the different sub-components of the debris population. While the difference between produced total quantities of smaller and larger debris particles may change at 10^{-3} m ($<10^{-3}$ m is dominated by small debris produced in debris collisions and ejecta, whereas $> 10^{-3}$ m is dominated by fragmentation and collision of larger bodies), it is also likely that as particle size increases the processes governing their evolution become more important. For larger particles, atmospheric drag and solar radiation pressure-related drag, such as Poynting-Robertson drag, have less effect; hence they have larger orbital lifetimes. Thus, the steeper regions of the curve, with smaller D_p, where the meteoroid flux is also a more significant portion

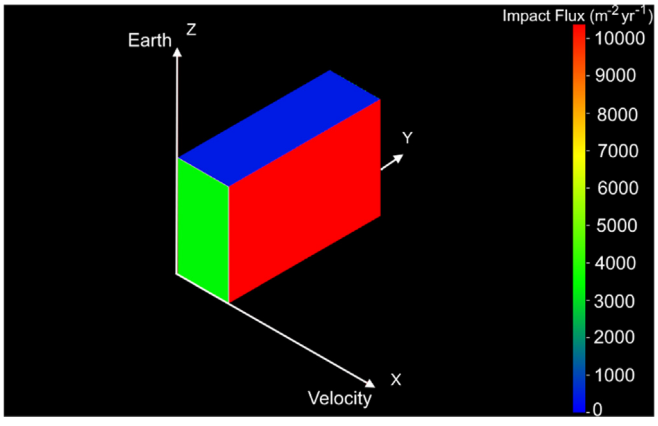

Fig. 5. 3-dimensional flux results for a 6U CubeSat in an orbit of 800 km altitude, inclination of 98.7°, and eccentricity of 0.0001, for an epoch of 1/11/2023–1/11/2026, produced by geometric analysis with ESABase2/Debris. The velocity vector is aligned with the x-axis and the Earth pointing vector is aligned with the Z-axis. The annual flux per m^2 per year is shown for particles of size from 1 μm to 1 cm.

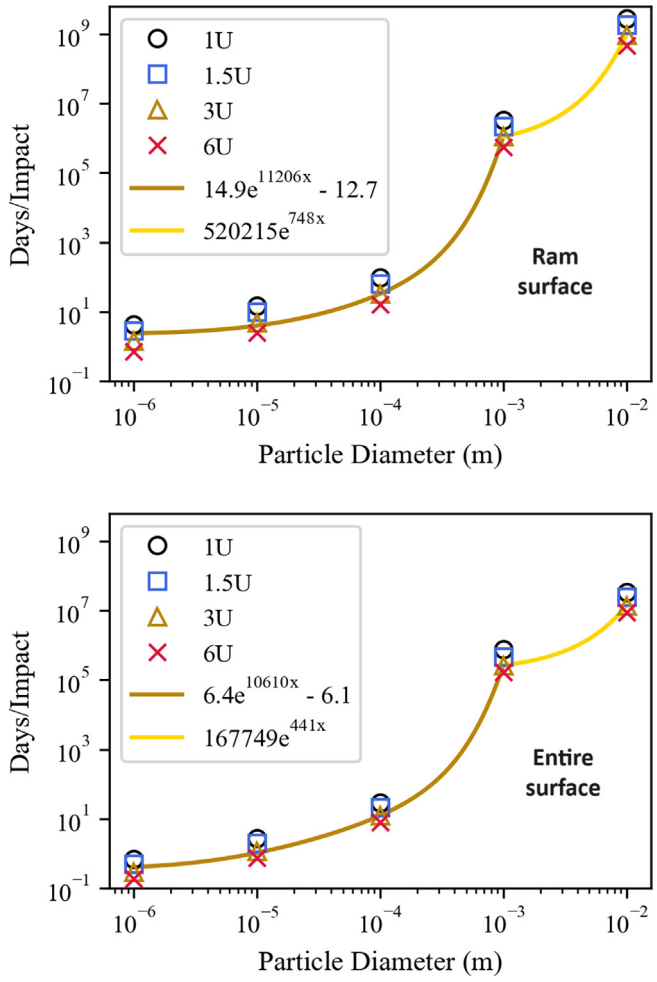

Fig. 6. The time in days expected before a particle (debris or dust) greater than a given size will impact the ram surface (top) and entire surface area (bottom) of a 1U, 1.5U, 3U, and 6U CubeSat in a circular orbit, with an inclination of 98.7° and altitude of 800 km (with the largest surface area face facing the ram direction). The 3U data is shown fitted. A single power law function does not fit the full data range, so separate fits are shown below and above particle diameters of 1 mm. This change in slope is a result of the rate of change of flux between the 1 mm and 1 cm-sized populations as debris begins to dominate over meteoroids (also see the change in slope of the total flux at a similar size in Fig. 4a).

of the overall flux, can be considered to be influenced by the production rate of such particles (supported by the meteoroid population continually being replenished/transient). Whereas the shallower region with greater D_p can be considered to be influenced by the long-term evolution of the orbits of the particles.

5.3. Discussion

The agreement between the flux derived from the discretised small plates from LDEF and the flux predicted by MASTER suggests that accumulating detection area over multiple small CubeSat face-sized plates, leads to statistically meaningful data over a time period of order 5 years, even at larger particle sizes with low fluxes per unit area where some of the small areas sampled might return null results. Here it is assumed that combining area over small plates separated by no more than tens of centimetres and covering no more than an area of 1.35 m x 1.07 m (the tray dimensions) is comparable to small detection surfaces separated within an orbit. This assumes in turn that the main component contributing to impacts is the average background population, and that this would be the same for plates separated by a small or large distance. This is based on the assumption that over time debris particles tend to distribute over the entire orbit (Kelso *et al.*, 2007). MASTER's input data comes from multiple separate missions, which implies a similar sample averaging, and MASTER uses statistical, deterministic, and probabilistic models to predict the particle environment. Meteoroid streams can be considered in MASTER; however, it is the background meteoroid flux that is dominant. Hence a background meteoroid flux model was used here (the Grün model with speed of 20 km s^{-1}), which includes an inherent averaging of seasonal streams. The final assumption is that we can then distribute the relevant detectors on a set of individual spacecraft distributed over an orbital region where the flux is unchanged, i.e. similar altitude but distributed along an orbit and in a variety of orbital planes.

Concerning the number of CubeSats required, the space exposed surface area considered here of 0.174 m^2 would represent seventeen single 1U faces. This could represent detectors on single faces of seventeen individual 1U CubeSats, or several detectors on various faces of three 6U CubeSats. However, considering the time before impact for millimetre-sized particles, the data in Fig. 6 would suggest that at least the entire surface area of one-hundred 6U CubeSats would be required to bring the observation time for a couple of impacts down to the order of 5 years, in-line with the operational lifetime for a typical CubeSat. This assumes either multiple faces per CubeSat are equipped with sensors, perhaps with SOLID, smart multi-layer insulation as flown on 'EQUilibriUm Lunar-Earth point 6U Spacecraft' EQUULEUS (Funase et al., 2020), or the use of telemetry data for impact detection (Bennett et al., 2021). Alternatively, large area thin films can be deployed such as with the Polyimide thin-film detector flown aboard 'Advanced Satellite Toward Exploration of dust enviRonment with In-Situ Cosmic dust sensor' ASTERISC (Ishimaru et al., 2021). It is clear from Table 2 that some technology types do indeed provide the same type of data as did SDS (i.e. flux, speed, direction), i.e. sufficient to not only obtain a flux but also orbital information on each object. If the data were to be collected from several viewing directions, the differences in the flux in each direction (which depends on the source) can be determined and compared to the various models.

Recently, many more CubeSat missions of $\geq$ 12U are being proposed for science missions that require greater payload space/power (e.g. Yu et al., 2018). Hosting smaller 1U–6U sized detectors on these bigger CubeSats and/or more traditional larger satellites, for which the extra mass

of the detector should be accommodatable, would be another efficient and sustainable way of accumulating the required detection area.

As stated, CubeSats are well known for being relatively cheap and having a quick time to launch and service, exemplified by ADLER-1, which went from idea to orbit in 1 year. With the greatly improved availability for launch, small CubeSats $\leq$ 6U could in principle provide a reactive debris monitoring response, ideal for monitoring the small particle debris environment produced in discrete events such as satellite collision and fragmentation events (accidental or deliberate). For a reactive launch, the period of time of maximum interest will need to be relatively short, in order to sample the produced debris before it spreads out over its orbit and begins to decay and evolve. Thus, even with larger effective detection areas, CubeSats used for such reactive missions would need to be well-targeted to intercept the predicted orbit of a particular stream of debris and to sample its full spatial extent, and the risk is that it is unlikely that enough CubeSats will be deployable with just traditional impact detectors, to provide sufficient detection area for larger particles.

In recent years, other (non-contact) approaches to detection have been suggested. These include bistatic radars (where the transmitter and receiver are separated and the target is a passive, non-cooperative object). For tracking larger debris such as inert satellites, the transmitter can be on the ground, the receiver on a CubeSat (at an altitude of say 400 km) and the tracked object (m scale size) at higher altitude such as 800 km. This does not however help track the mm-sized debris that is the critical risk – this would require a radar transmitter on the CubeSat. In theory, radar systems be reduced in size and placed onto a CubeSat to track 1 mm sized debris at 100 m range, greatly increasing the sampled volume and promising daily detection objects at typical LEO fluxes, although this remains to be demonstrated (Ahmed et al., 2019). The recent ADLER-2 launch (July 2023) carried such a radar system (Austrian Space Forum, 2023), and a demonstration of its capabilities is awaited. Other systems to enhance the effective area have also been proposed. STRATCHcube (Creed et al., 2021), also has a radar included in its design. There are also laser sheet based optical systems (Englert et al., 2014), optical systems such as CubeSat star trackers (Dave et al., 2022), the use of telemetry data for impact (Bennett et al., 2021), etc.

It should be noted that beam-park radar campaigns from the ground can provide statistical data on cm-sized objects in LEO (e.g. 3.5 cm at 700–1000 km altitude and 5 cm at 1300 – 1600 km, Muntoni et al., 2021). Indeed the Russian deliberate destruction of Cosmos-1408 in 2021, permitted a test of beam-park tracking, where the origin of the debris was known in space and time, as well as the parameters obtained during the observation campaign. By making various assumptions, the debris field of Cosmos-1498 could be tracked and orbital data obtained for particles over approximately 3 cm size (Kastinen et al., 2023).

6. Conclusions

The danger posed by space debris to continued successful operation of spacecraft in LEO is a real one. The risk analysis here in Section 2, shows that, at low altitudes this risk is currently worse for 1–10 mm sized debris. One can always improve Table 1 and Fig. 1, which show this risk. A greater range than 1 – 10 can be used to allocate scores for example, fine-tuning the ranking. Moreover, some observers may judge the scores slightly differently – this is subjective. However, as long as you combine a falling curve (flux) with a rising curve (impact consequence) there will be a peak at some crossover region. Further, the picture is not static. As more and more satellites are launched, then at some altitudes the flux for impacts between whole spacecraft themselves (m to 10 s of m-scale) will increase and may even become the dominant risk. Since this will trigger a large volume of smaller debris, the hazard due to mm-scale impactors will then increase further, which can in turn trigger further debris release, etc., generating the long predicted runway scenario of the Kessler syndrome (Kessler and Cour-Palais, 1978).

The colour coded hazard-flux curve shown in Fig. 1 is thus not the final answer – it will change with time. For example, in the 1950s, there would have been no debris contribution to the flux, so the hazard will have been lower at the size scales now dominated by debris (as is the case at the Moon today for example). Further, over the next decade or so, more of the curve will become red (high risk) as more mm and m scale debris objects populate LEO. The colour coding will also change dependent on the orbit under consideration. For example, LEO covers a wide range of altitudes, some of which (e.g., sun-synchronous orbits are 800 km) are more favoured than others – if ever-increasing numbers of satellites cluster in such orbits, the risk there will increase. Evidence that this hazard is increasing is given by the ever-greater frequency of orbital avoidance manoeuvres being carried out by spacecraft in LEO.

The need to monitor the flux of objects is thus evident. Whilst this can be done fairly well from the ground for objects of cm scale and above, as indicated, it is more problematic at the mm-scale, and needs in-situ measurement. The various techniques required for this include many that can be hosted on CubeSats. This offers an alternative to the single instrument on a large satellite model often used in the past. Provided that is, both the cost and scientific effectiveness of a distributed network of sensors mounted on a fleet of CubeSats can be shown to be satisfactory. This has been demonstrated in the later sections of the paper, where a network of up to order 100 CubeSats and impact detectors can be both cost-effective, and deliver a flux measurement at the 1 mm scale on a time-scale of around 5 years.

A final issue with the CubeSat revolution is: Who pays? Payloads on scientific spacecraft are traditionally developed and paid for by a space agency. The data is then processed and published (after peer-review) in the scientific literature and subsequently incorporated into software tools distributed by the agencies. The CubeSat revolution (combined with generally lower launch costs per kg) challenges this model. In the case here, a commercial company could provide the dust flux instruments needed and arrange their launch on multiple CubeSats. They would then have to collect data over a period of years and process it. How to monetize this activity is still unclear. One route is for a major space agency to purchase the measurements as a service from industry. Validation of the data quality would still be required, as would its subsequent incorporation into the flux modelling tools provided by said agency (usually via a contract to industry). A variation on this would be for the commercial provider to generate their own flux model and provide it as a bolt on extra to a pre-existing modelling tool, with license fees for its use. Either way, the results presented here show that whilst it is feasible to provide a meaningful flux from CubeSat based impact detectors, a large number of CubeSats will need to be used to obtain the flux for 1 mm sized particles and the data collection period will last several years. Thus, any financial model would thus have to extend over that period. However, total costs, data quality, time to construct and launch, can be better than those for traditional, large scale single missions, thus potentially closing the worrying data gap for space debris of 1 mm size. It could of course be argued that the deployment in LEO of these CubeSats would itself constitute a debris hazard. However, the numbers are still small compared to the number of satellites already deployed in this volume of space, and if the impact detectors can be hosted on spacecraft performing other tasks as well, the extra contribution to the debris hazard is minimised. Of course, the hosting spacecraft will need to comply rigorously with end of life deorbiting strategies, and it would indeed be ironic if in providing the necessary data to monitor this hazard, the use of CubeSats led to a real impact incident.

Declaration of interest

Regarding the manuscript submission titled *'Feasibility of using CubeSats and Small Detectors for In-situ Space Debris and Cosmic Dust Flux Measurement'* by Luke T. Cornwell, Mark J. Burchell, Penelope J. Wozniakiewicz, the authors declare that there are no competing interests to declare.

Acknowledgements

GNOSIS (STFC) is thanked for a grant that helped fund LC's PhD studentship.

Data and code availability

The authors confirm that all the data used in the work is included in this paper. The details necessary to run the MASTER and ESABase2 software to reproduce the results are also given.

The software used in this work (MASTER-8.0.3) is freely downloadable from ESA at the ESA Space Debris User Portal https://sdup.esoc.esa.int/. The ESABase2/Debris software is licensed by Etamax Space GmbH, and is downloadable from Fev Etamax at https://esabase2.net.

References

Ahmad, S., 2021. Anti-satellite test: from the perspective of international space law and the law of armed conflict. Inter. Crimin. Law Rev. 21, 342–366. https://doi.org/10.1163/15718123-BJA10046.

Ahmed, R., Majurec, N. and De Bleser, J., 2019. A CubeSat-based radar for characterization of millimetric orbital debris. Presented at: 1st Int. Orbital Debris Conf., Texas., USA (Dec. 2019). Abstract 6079 (9pp). https://www.hou.usra.edu/meetings/orbitaldebris2019/orbital2019paper/pdf/6079.pdf.

Anz-Meador, P., Ward, M., Manis, A., Nornoo, K., Dolan, B., Claunch, C., and Rivera, J., 2019. The Space Debris Sensor Experiment. Presented at: 1st Int. Orbital Debris Conf., Texas, USA (Dec. 2019), 10pp. https://ntrs.nasa.gov/citations/20190033909.

Anz-Meador P., Opiela J., and Liou, J.C., 2022. History of On-orbit Satellite Fragmentations, 16th Edition. NASA/TP-20220019160 (716 pp). https://orbitaldebris.jsc.nasa.gov/library/hoosf_16e.pdf.

Austrian Space Forum, 2023. ADLER-1-2 (2023). https://adler.oewf.org/. Site accessed Jan. 2024.

Bauer, W., Romberg, O., Krag, H., et al., 2016. Debris in-situ impact detection by utilization of cube-sat solar panels. Presented in the 4S Symposium 2016, Malta, (pp. 11). https://www.montenegros.de/sergio/public/4s-2016-solid.pdf.

Bauer, W., 2021. SOLID-A solar panel based impact detector. in From Measurements to Understanding: Presented in 1st MASTER Modeling Workshop, ESA ESOC (Darmstadt, Germany), 2021, pp. 18, https://indico.esa.int/event/370/timetable/?view=standard (Accessed 10/05/2023).

Bennett, A.A., Schaub, H., Carpenter, R., 2021. Assessing debris strikes in spacecraft telemetry: Development and comparison of various techniques. Acta Astronaut. 181, 516–529. https://doi.org/10.1016/j.actaastro.2020.09.009.

Brumbaugh, K.M., Kjellberg, H.C., Glenn Lightsey, E., Wolf, A., Laufer, R., 2012. In-situ sub-millimeter space debris detection using cubesats. Adv. Astronaut. Sci. 144, 789–803 https://www.univelt.com/book=5286.

CalPoly, 2022. California Polytechnic State University. Cubesat Design Specification Rev 14.1. 34 (2022).

Carpenter, J.D., Wells, A., Abbey, A.F., Ambrosi, R.M., 2008. Meteoroid and space debris impacts in grazing-incidence telescopes. A&A 483, 941–947. https://doi.org/10.1051/0004-6361:200809414.

Caswell, R.D., McBride, N., Taylor, A., 1995. Olympus end of life anomaly — a perseid meteoroid impact event? Adv. Space Res. 17, 139–150. https://doi.org/10.1016/0734-743X(95)99843-G.

Christiansen, E.L., 1993. Design and performance equations for advanced meteoroid and debris shields. Int. J. Impact Eng. 14, 145–156. https://doi.org/10.1016/0734-743X(93)90016-Z.

Colombo, C., Trisolini, M., Scala, F. et al., 2021. E.CUBE MISSION : The environmental cubesat. In 8th European Conference on Space Debris, Darmstadt, Germany (2021), 9pp. Ed. T. Flohrer, S. Lemens & F. Sschmitz. Pub. ESA Space Debris Office. https://conference.sdo.esoc.esa.int/proceedings/sdc8/paper/309.

Cooke B., 2014. Meteoroid Induced Anomalies on Spacecraft. Presented at the Space Anomalies and Failures Workshop, Virginia, USA, May 2014, 26 pp. https://ntrs.nasa.gov/api/citations/20140012583/downloads/20140012583.pdf Site accessed Sept. 2023.

Cornwell, L.T., Wozniakiewicz, P.J., Burchell, M.J., et al., 2023. A study on the capabilities and accuracy of Kapton based TOF space dust and debris detectors. Adv. Sp. Res. 72, 2959–2970. https://doi.org/10.1016/j.asr.2022.07.022.

Cour-Palais, B.G., 1987. Hypervelocity impact in metals, glass and composites. Int. J. Impact Eng. 5, 221–237. https://doi.org/10.1016/0734-743X(87)90040-6.

Creed, L., Graham, J., Jenkins, C., et al., 2021. STRATHcube: The Design of a CubeSat for Space Debris Detection Using In-Orbit Passive Bistatic Radar. Presented at: 72nd International Astronautical Congress (IAC), Dubai, UAE, 2021. pp. 8. IAC-21,A6,1,2,x66530. https://pure.strath.ac.uk/ws/portalfiles/portal/130341788/Creed_etal_IAC_2021_STRATHcube_the_design_of_a_CubeSat_for_space_debris_detection.pdf.

Dave, S. and Lee, R.S.K., 2022. Feasibility of a Virtual Constellation using Small Aperture , Wide Field of View Optical Systems for Space Domain Awareness and Applications. Presented at the Advanced Maui Optical and Space Surveillance Technologies Conference 2022 (AMOS 2022 Technical Papers). pp. 13. https://amostech.com/TechnicalPapers/2022/Poster/Dave.pdf.

Della Corte, V., Ferretti, S., Piccarillo, A.M., et al., 2023. DISC - the Dust Impact Sensor and Counter on-board Comet Interceptor: characterization of the dust coma of a dynamically new comet. Adv. Sp. Res. 71, 3457–3467. https://doi.org/10.1016/j.asr.2023.01.049.

Dignam, A., Wozniakiewicz P., Burchell M., et al., 2022. Palladium-coated Kapton for use on dust detectors in low Earth orbit: Performance under hypervelocity impact and atomic oxygen exposure. Frontiers in Space Technology 3:933664. (14 pp.) https://doi.org/10.3389/frspt.2022.933664.

D-Orbit Space, 2023. https://www.dorbit.space/above-the-sky-june-2023 Site accessed 7/10/23.

Drolshagen, G., Svedhem, H., Grün, E., Grafodatsky, O., Prokopiev, U., 1999. Microparticles in the geostationary orbit (GORID experiment). Adv. Space Res. 23 (1), 123–133. https://doi.org/10.1016/S0273-1177(98)00239-7.

Englert, C.R., Bays, J.T., Marr, K.D., et al., 2014. Optical orbital debris spotter. Acta Astronaut. 104, 99–105. https://doi.org/10.1016/j.actaastro.2014.07.031.

ESA, 2023a. ESA Space Debris Office. ESA ' s Annual Space Environment Report. https://www.sdo.esoc.esa.int/environment_report/Space_Environment_Report_latest.pdf (2023).

ESA, 2023b. ESA's Space Debris Office. Space debris by the numbers. www.esa.int/Space_Safety/Space_Debris/Space_debris_by_the_numbers (2023).

ESA, 2023c. ESA Space Debris User Portal. https://sdup.esoc.esa.int/ (Accessed 10.05.23).

Faure, P., Masuyama, S., Nakamoto, H., et al., 2013. Space dust impacts detector development for the evaluation of ejecta. Procedia Eng. 58, 594–600. https://doi.org/10.1016/j.proeng.2013.05.068.

FCC, 2022. FCC Adopts 5-Year Rule (Space Innovation IB Docket No. 22-271 Mitigation of Orbital Debris in the New Space Age IB Docket No. 18-313) 2022. https://docs.fcc.gov/public/attachments/FCC-22-74A1.pdf. Site accessed Jan. 2024.

FEV, 2023. FEV Etamax GmbH. ESABase2. https://esabase2.net. Accessed 10.05.23.

Funase, R., Ikari, S., Miyoshi, K., et al., 2020. Mission to Earth-Moon Lagrange Point by a 6U CubeSat: EQUULEUS. IEEE Aerosp. Electron. Syst. Mag. 35, 30–44. https://doi.org/10.1109/MAES.2019.2955577.

Furumoto, M., Sahara, M., 2020. Statistical assessment of detection of changes in space debris environment utilizing in-situ measurements. Acta Astronaut. 177, 666–672. https://doi.org/10.1016/j.actaastro.2020.08.011.

Goel, A., Krishnamoorthy, S., Swenson, T., et al., 2017. Design for CubeSat-based dust and radiation studies at Europa. Acta Astronaut. 136, 204–218. https://doi.org/10.1016/j.actaastro.2017.03.016.

Graps A.L., Green S.F., McBride N.M., McDonnell J.A.M., Bunte K.D., Svedham H., Drolshagen G., 2007. GEO debris and interplanetary dust: fluxes and charging behaviour. In: Krueger, H. and Graps, A. L. eds. Dust in Planetary Systems. ESA SP-643. ESTEC, Noordwijk, The Netherlands: ESA Publications Division, pp. 97–102.

Groemer, G., & Stumptner, W., 2021. ADLER-1 Austrian Debris Detection Low Earth (orbit) Reconnoiter. in From Measurement to understanding. Presented in 1st MASTER Modeling Workshop, ESA ESOC (Darmstadt, Germany), 2021. pp. 8. https://indico.esa.int/event/370/timetable/?view=standard (Accessed 10/05/2023).

Grün, E., Krüger, H., and Srama, R., 2019. The Dawn of Dust Astronomy. Space Sci. Rev. 215:46. https://doi.org/10.1007/s11214-019-0610-1.

Grün, E., Gustafson, B.Å.S., Dermott, S.F., Fechtig, H. (Eds.), 2001. Interplanetary Dust. Springer, Pub.

Hamilton, J., Liou, J.C., Anz-Meador, P., et al., 2017. Development of The Space Debris Sensor. In: Schmitz, T., Flohrer, F. (Eds.), Proceedings of the 7th European Conference on Space Debris. Pub. ESA Space Debris Office, 11 Pages. URL: https://conference.sdo.esoc.esa.int/proceedings/sdc7/paper/965.

Hirai, T., Cole, M.J., Fujii, M., et al., 2014. Microparticle impact calibration of the Arrayed Large-Area Dust Detectors in INterplanetary space (ALADDIN) onboard the solar power sail demonstrator IKAROS. Planet. Space Sci. 100, 87–97. https://doi.org/10.1016/j.pss.2014.05.009.

Hörz, F., Bernard, R.P., Warren, J., et al., 1991. Preliminary Analysis of LDEF Instrument A0187-1 "Chemistry of Micrometeoroids Experiment. In: LDEF-69 Months in Space First Post-retrieval Symposium Part-1 (ed. Levine, A. S.) p. 478–501 (NASA Conference Publication 3134). https://ntrs.nasa.gov/api/citations/19920014072/downloads/19920014072.pdf.

Hörz, F., Bernhard, R.P., See, T.H., 1995. Hypervelocity penetration in aluminum 6061 and 1100 alloys. In: Murr, L.E., Staudhammer, K.P., Meyers, M.A. (Eds.), *Metallurgical and materials applications of shock-wave and high-strain-rate phenomena*. Elsevier Science B.V, pp. 273–283.

Humes, D. H., 1993. Small Craters on The Meteoroid and Space Debris Impact Experiment. In: LDEF - 69 Months in Space Third Post-Retrieval Symposium Part 1 (ed. Levine, A. S.) p. 287–322 (NASA Conference Publication 3275).

IADC-2023, 2023. IADC-04-03, Protection Manual ver. 7.2, 2023. https://iadc-home.org/documents_public/view/id/288#u Site accessed Jan. 5th, 2024.

Ishimaru R., Sakamoto Y., Fujita S., Kobayashi M., Okudaira O., Maeda K., Kimura H. and Matsui T., 2021. Asterisc Project: Cubesat Mission For Observation Of Cosmic Dust With A New Large Film Type Dust Sensor. 52nd Lunar and Planetary Science Conference, Houston, Tx, USA, 2021 (LPI Contrib. No. 2548) abstract #1712. https://www.hou.usra.edu/meetings/lpsc2021/pdf/1712.pdf.

Johnson, N.L., 2021. Operation Burnt Frost: A View From Inside. Space Policy 56101411. https://doi.org/10.1016/j.spacepol.2021.101411.

Kastinen, D., Vierinen, J., Grydeland, T., Kero, J., 2023. Using radar beam-parks to characterize the Kosmos-1408 fragmentation event. Acta Astronaut. 202, 341–359. https://doi.org/10.1016/j.actaastro.2022.10.021.

Kelso, T. S., 2007. Analysis of the 2007 Chinese ASAT Test and the Impact of its Debris on the Space Environment. In: Advanced Maui Optical and Space Surveillance Technologies Conference (AMOS 2007), Maui, Hawaii, September 2007. Ed.: S. Ryan. 10 pp. https://celestrak.org/publications/AMOS/2007/AMOS-2007.pdf.

Kessler, D.J., Cour-Palais, B.G., 1978. Collision frequency of artificial satellites: The creation of a debris belt. J. Geophys. Res. 83 (A6), 2637–2646. https://doi.org/10.1029/JA083iA06p02637.

Kessler, D.J., Reynolds, R.C., Anz-meador, P.D., 1989. Orbital Debris Environment for Spacecraft Designed to Operate in Low Earth Orbit.

NASA Tech. Memo. 100 471, 22 pages https://apps.dtic.mil/sti/citations/ADA339021.

Liou, J., Giovane, F.J., Corsaro R., *et al.*, 2006. LAD-C : A large area debris collector on the ISS. In 36th COSPAR General Assembly, Beijing, China, 2006, pp. 7. https://ntrs.nasa.gov/api/citations/20060028448/downloads/20060028448.pdf.

Liou, J.-C., Johnson, N.L., 2006. Risks in space from orbiting debris. Science 31 (5759), 340–341. https://doi.org/10.1126/science.1121337.

Liu Z. Cao W., Zhang W., Chi R., Pang B., Yang N., 2021. Double Layered 2-D Pvdf Film Based Flexible Sensor For Detection Of Micro-Space-Debris: Impact Velocity, Angle, And Spot. 2020 15th Symposium on Piezoelectrcity, Acoustic Waves and Device Applications (SPAWDA), Zhengzhou, Henan Province, China, pp. 366-370, doi: 10.1109/SPAWDA51471.2021.9445541.

Love, S.G., Brownlee, D.E., King, N.L., Hörz, F., 1995. Morphology of meteoroid and debris impact craters formed in soft metal targets on the LDEF satellite. Int. J. Impact Engng. 16, 405–418. https://doi.org/10.1016/0734-743X(94)00050-7.

McDonnell, J.A.M., 1987. The Giotto dust impact detection system. J. Phys. e. 20, 741–758. https://doi.org/10.1088/0022-3735/20/6/033.

Menzel, M., Davis, M., Parrish, K., et al., 2023. The Design, Verification, and Performance of the James Webb Space Telescope. Publications of the Astronomical Society of the Pacific 135, 058002 (42pp). https://doi.org/10.1088/1538-3873/acbb9f.

Muntoni, G., Montisci, G., Pisanu, T., Andronico, P., Valente, G., 2021. Crowded space: a review on radar measurements for space debris monitoring and tracking. Appl. Sci. 11, 1364. https://doi.org/10.3390/app11041364.

NASA FY2022, 2022. NASA Congressional Budget Justification, 2022. https://www.nasa.gov/sites/default/files/atoms/files/fy2022_congressional_justification_nasa_budget_request.pdf Website accessed Sept. 2023.

NASA ODQN, 2010. NASA Orbital Debris Newsletter 14(2), 1 – 3, 2010. https://orbitaldebris.jsc.nasa.gov/quarterly-news/pdfs/odqnv14i2.pdf Website accessed Sept. 2023.

NASA ODQN, 2020. Orbital Debris Program Office, Orbital Debris Quarterly News. 24(1), 4 - 8 (2020). https://orbitaldebris.jsc.nasa.gov/quarterly-news/pdfs/ODQNv24i1.pdf Site accessed Oct. 2023.

NASA SOA-2022. Deorbit Systems. https://www.nasa.gov/smallsat-institute/sst-soa/deorbit-systems/. Site accessed Sept. 2023.

NASA, 2021. NASA'S EFFORTS TO MITIGATE THE RISKS POSED BY ORBITAL DEBRIS, Report No. IG-21-011. Office of the Inspector General, NASA Office of Audit, US, 2021. https://www.oversight.gov/sites/default/files/oig-reports/NASA/IG-21-011.pdf.

NASA-DM, 2023. NASA-DM, Debris Mitigation, 2023. https://www.orbitaldebris.jsc.nasa.gov/mitigation/ Website accessed Sept. 2023.

NRC 2011. National Research Council. Limiting Future Collision Risk to Spacecraft: An Assessment of NASA's Meteoroid and Orbital Debris Programs. Washington, DC: The National Academies Press (2011). https://doi.org/10.17226/13244.

O'Neal, R. L. & Lightner, E.B., 1991. Long Duration Exposure Facility-A General Overview. In: LDEF-69 Months in Space First Post-retrieval Symposium Part 1 (ed. Levine, A.) p. 3–48. NASA Conference Publication 3134. https://ntrs.nasa.gov/api/citations/19920014037/downloads/19920014037.pdf.

ODIN Space, 2023. https://www.odin.space. Site accessed 7/10/23.

Oikonomidou, X., Karagiannis, E., Still, D., *et al.*, 2022. MOVE-III : A CubeSat for the detection of sub-millimetre space debris and meteoroids in Low Earth Orbit. Front. Sp. Technol. 1–18. doi:10.3389/frspt.2022.933988.

Pardini, C., Anselmo, L., 2009. Assessment of the consequences of the Fengyun-1C breakup in low Earth orbit. Adv. Space Res. 44, 545–557. https://doi.org/10.1016/j.asr.2009.04.014.

Pardini, C., Anselmo, L., 2023. The short-term effects of the Cosmos 1408 fragmentation on neighboring inhabited space stations and large constellations. Acta Astronaut. 210, 465–473. https://doi.org/10.1016/j.actaastro.2023.02.043.

Schimmerohn, M., Ledford, N., Putzar, R., *et al.*, 2021. LARID: Concept of a large area low resource integrated impact detector. Presented at the 19th IAA SYMPOSIUM ON SPACE DEBRIS (A6) Space Debris Detection, Tracking and Characterization - SST (1), Dubai (UAE). 2 pages. https://iafastro.directory/iac/paper/id/63926/summary/.

Schwanethal, J. P., McBride, N., Green, S. F., McDonnell, J. A. M. & Drolshagen G., 2005. Analysis of impact data from the debie (Debris In-Orbit Evaluator) sensor in polar low earth orbit. Proceedings of the Fourth European Conference on Space Debris, Darmstadt, Germany, 18-20 April 2005 (ESA SP-587). https://conference.sdo.esoc.esa.int/proceedings/sdc4/paper/102/SDC4-paper102.pdf.

See, T., Allbrooks, M., Atkinson, D., Simon, C. and Zolensky, M., 1990. Meteoroid and Debris Impact Features Documented on the Long Duration Exposure Facility. pp. 598. https://apps.dtic.mil/sti/pdfs/ADA337849.pdf.

Snodgrass, C., Jones, G.H., 2019. The European Space Agency's Comet Interceptor lies in wait. Nat. Commun. 10, 5418. https://doi.org/10.1038/s41467-019-13470-1.

Sordini, R., Della Corte, V., Rotundi, A., et al., 2018. GIADA performance during Rosetta mission scientific operations at comet 67P. Adv. Sp. Res. 62, 1987–1997. https://doi.org/10.1016/j.asr.2017.07.031.

Space.Com, 2023. https://www.space.com/starlink-satellite-conjunction-increase-threatens-space-sustainability Site accessed, Oct. 12, 2023.

Strüder, L., Aschenbach, B., Bräuninger, H., Drolshagen, G., Englhauser, J., Hartmann, R., Hartner, G., Holl, P., Kemmer, J., Meidinger, N., Stübig, M., Trümper, J., 2001. Evidence for micrometeoroid damage in the pn-CCD camera system aboard XMM-Newton. A&A 375, L5–L8. https://doi.org/10.1051/0004-6361:20010916.

TASS, 2023. https://tass.com/science/1580279 Site accessed Oct. 12, 2023.

Tuzzolino, A.J., McKibbin, R.B., Simpson, J.A., et al., 2001. The Space Dust (SPADUS) instrument aboard the Earth-orbiting ARGOS spacecraft: II–results from the first 16 months of flight. Planet. Space Sci. 49, 705–729. https://doi.org/10.1016/S0032-0633(01)00013-7.

Tuzzolino, A.J., Economou, T.E., McKibben, R.B., Simpson, J.A., McDonnell, J.A.M., Burchell, M.J., Vaughan, B.A.M., Tsou, P., Hanner, M.S., Clark, B.C., Brownlee, D.E., 2003. Dust flux monitor instrument for the stardust mission to comet wild 2. J. Geophys. Res **E** 108 (E10), 8115. https://doi.org/10.1029/2003JE002086.

UK Stats, 2023. UK Office of National Statistics CPI Index. https://www.ons.gov.uk/economy/inflationandpriceindices/timeseries/l522/mm23 accessed 7/10/2023.

Warren, J.J., Cole, M., Offenberger, S., Kota, K.R., Lacy, T.E., Toghiani, H., Burchell, M., Kundu, S., Pittman Jr., C.U., 2021. Hypervelocity impacts on honeycomb core sandwich panels filled with shear thickening fluid. Inter. J. Impact Eng. 150103803. https://doi.org/10.1016/j.ijimpeng.2020.103803.

Watts, A., Atkinson, D., Rieco, S., 1993. Dimensional scaling for impact cratering and perforation. Int. J. Impact Eng. 17, 925–935. https://doi.org/10.1016/0734-743X(95)99911-A.

Wozniakiewicz, P.J., Burchell, M.J., 2019. Space dust and debris near the Earth. Astron. Geophys. 60, 38–42. https://doi.org/10.1093/astrogeo/atz150.

Wozniakiewicz, P., 2017. Cosmic dust in space and on Earth. Astron. Geophys. 58, 1.35–1.40. https://doi.org/10.1093/astrogeo/atx027.

Yu, X., Zhou, J., Zhu, P., Guo, J., 2018. Star of AOXiang: An innovative 12U CubeSat to demonstrate polarized light navigation and microgravity measurement. Acta Astronaut. 147, 97–106. https://doi.org/10.1016/j.actaastro.2018.03.014.